A global-local finite element analysis of hybrid composite-to-metal bolted connections used in aerospace engineering

Liang, Ke

DOI
10.1007/s11771-017-3526-5

Publication date
2017

Document Version
Final published version

Published in
Journal of Central South University

J. Cent. South Univ. (2017) 24: 1225−1232
DOI: 10.1007/s11771-017-3526-5

Springer

A global-local finite element analysis of hybrid composite-to-metal bolted connections used in aerospace engineering

LIANG Ke(梁珂)[1, 2]

1. Qian Xuesen Laboratory of Space Technology, China Academy of Space Technology, Beijing 100094, China;
2. Faculty of Aerospace Engineering, Delft University of Technology, Delft 2629HS, the Netherlands

Abstract: Efficient bolted joint design is an essential part of designing the minimum weight aerospace structures, since structural failures usually occur at connections and interface. A comprehensive numerical study of three-dimensional (3D) stress variations is prohibitively expensive for a large-scale structure where hundreds of bolts can be present. In this work, the hybrid composite-to-metal bolted connections used in the upper stage of European Ariane 5ME rocket are analyzed using the global-local finite element (FE) approach which involves an approximate analysis of the whole structure followed by a detailed analysis of a significantly smaller region of interest. We calculate the Tsai-Wu failure index and the margin of safety using the stresses obtained from ABAQUS. We find that the composite part of a hybrid bolted connection is prone to failure compared to the metal part. We determine the bolt preload based on the clamp-up load calculated using a maximum preload to make the composite part safe. We conclude that the unsuitable bolt preload may cause the failure of the composite part due to the high stress concentration in the vicinity of the bolt. The global-local analysis provides an efficient computational tool for enhancing 3D stress analysis in the highly loaded region.

Key words: bolted connection; global-local finite element approach; failure; bolt preload

1 Introduction

Composite materials are increasingly used in engineering applications because of their high specific strength [1]. The implementation of composite materials in conjunction with metals into hybrid structural systems is currently being developed in several key applications, especially in the aerospace engineering field. Synergistic effect and economical design are often achieved in a hybrid structure, compared to a single material system. However, the design of the hybrid joint presents a greater challenge than that found in joining similar materials, mainly due to the differences in the constituent material properties [2−5]. The mismatch in the coefficients of thermal expansion and moisture absorption causes differential strain between the metal and composite parts [5]. The bolt clamp-up load may be compromised by bolt stress relaxation due to viscoelastic creep of the composite, which has been studied by SUN et al [6] and CACCESE et al [7, 8]. Maintaining adequate bolt clamp-up load can significantly affect the strength of the connection. PARKES et al [9] presented a novel metal-composite joining technology to analyze the static strength of the hybrid connection. Hybrid composite-metal bolted connections are also susceptible to the fatigue life of the metal. STARIKOV and SCHON [10] and KELLY [11] applied the experimental and numerical study on fatigue of composite-metal bolted joints.

Analysis and design of strong and durable hybrid joints are now recognized as an engineering problem of prime importance. The mechanical response of hybrid composite-to-metal bolted joints can be complex due to the interactions between the several joint parts, the step-wise geometry variation, the inherent complexity of composite materials, the junction of materials with dissimilar properties and the various parameters which can influence the joint behavior. The stress analysis of the hybrid bolted connection shows some distinctive features as the 3D nature of the stress fields, extremely high stress gradients, and mathematical stress singularities at certain points/lines of the structure. Hence, application of three-dimensional (3D) solid finite elements [12, 13] in numerical analysis of composite-metal bolted connections gains increasing interests. Various 3D finite element analysis approaches have been applied to the bonded joints in Refs. [14, 15]. IREMAN [16] proposed a model for a detailed study of the behavior, strength and stress distribution in composite bolted joints using 3D finite element model. TSERPES

Foundation item: Project(282522) supported by the European Union's Research and Innovation Funding Programme
Received date: 2016−02−22; **Accepted date:** 2016−05−23
Corresponding author: LIANG Ke, Associate Professor, PhD; Tel: +86−18392957817; E-mail: liangke.nwpu@163.com

et al [17] considered the clearance between bolts and holes in the study of joints with protruding fasteners based on Ireman's model. The progressive damage analysis of composite bolted joints has been studied by HUHNE et al [18] using a 3D model. This research showed the potential for a sufficiently detailed 3D FE model to capture the local and global effects of geometrical features and parameters on mechanical response of the joints. Bolted connections are extensively used in structures where the ability to easily remove structural components is required, such as the large-scale structures used in aircrafts and rockets where hundreds of bolts may be needed. Using 3D solid elements to model this kind of complex structures is technically complicated or even impossible, and in addition, the corresponding 3D stress analysis results in the occupation of long CPU time and large storage space. A possible alternative to reduce the modeling and computational complexity without compromising the accuracy of the results is the global-local analysis [19−22], where a smaller zone of interests is reanalyzed after an approximate analysis of the entire structure. Global-local finite element approaches have been generally used to manage 3D stress analysis in the case of bonded joints. A 27-node hexahedral solid element has been implemented into the sub-modeling function of ABAQUS for the 3D stress analysis of composite-to-aluminum bonded joints [23]. BOGDANOVICH and KIZHAKKETHARA [24] used a global-local type sub-modeling approach with this 27-node solid element of ABAQUS to analyze the double-lap composite bonded joints with adhesive layers. LIU et al [25] investigated the technique to deal with the non-matching interface in global-local algorithm.

Ariane 5ME is a European heavy lift launch vehicle that is a part of the Ariane rocket family. The composite cap and the aluminum ring are connected on flanges using 120 bolts along the circumference in the upper stage of an evolved design for a mid-life upgrade of Ariane 5ME. In this work, a global-local finite element analysis of these hybrid composite-to-metal bolted connections is carried out. A two-dimensional (2D) structural analysis based on the shell element typology is used for the global model. The initial design of the global model is provided by Dutch space center and eight thermo-mechanics load cases are applied sequentially to approximate the expected flight scenario. According to the stress results of the global model, the most highly loaded region along the circumference, called the local model, is selected and modeled using the 3D solid elements. The 3D stress analysis and the failure prediction are applied for the most critical region.

The outline of this work is as follows. The detailed description of the structure analyzed in this work is showed in Section 2. The global-local finite element approach used in this study is introduced in Sections 3. The numerical results obtained are presented in Section 4, and based on these results, an improvement design is achieved in Section 5. We summarize the work and draw conclusions in Section 6.

2 Description of structure

A composite cap has been designed as a lower weight alternative for the lower end of the engine thrust frame of the Ariane 5ME in Dutch space center, as shown in Fig. 1. The composite cap is at the bottom of the aluminum cone and is rotated to obtain a better viewing. The cone and the cap are combined to be the global structure (Fig. 2(a)) which will be analyzed in this work. The upper circumference of the conical cap ends in a flange which is bolted to the aluminum bottom ring of the cone. One of the 120 composite-to-metal bolted connections is shown in Fig. 2(b), which is composed of three parts, the composite part from the cap flange, the aluminum box from the ring of the cone and the steel bolt. An evaluation of the bolted connection of the composite and aluminum flanges in that region is required.

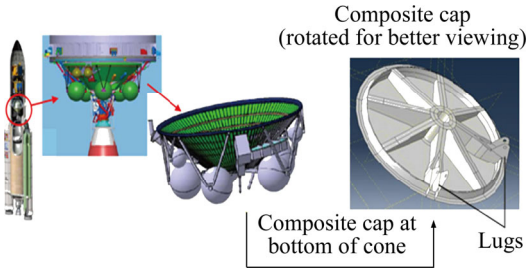

Fig. 1 Composite cap in upper stage of Ariane 5ME

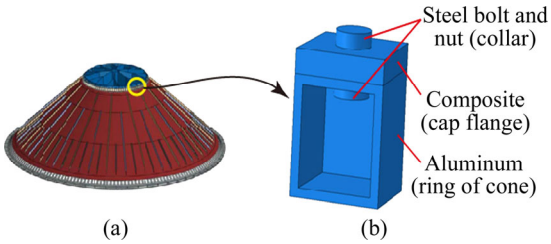

Fig. 2 Sketch of global model and one of composite-to-metal bolted connection models: (a) Global model (upside-down for clarity); (b) One of 120 bolted connections

3 Approach used

A global-local finite element approach is used in the framework of the commercial software ABAQUS. First, the global finite element model is constructed. Then, the eight thermo-mechanical load conditions are applied sequentially and the most highly loaded region along the circumference is determined. A local finite element

model of the critical region, including a model of the bolt, is then created for a detailed evaluation.

3.1 Global-local FE model

The global-local analysis is performed in two steps.

In the first step, the global finite element model is constructed using 59206 two-dimensional shell elements S4R with 4 nodes, as shown in Fig. 3(a). The flanges of the composite cap and aluminum ring are modeled with coincidental nodes that allow separation and contact, where the contact type termed hard contact is used. The elastic-plastic analysis and the geometric nonlinearity are both considered in the stress analysis of the global model.

The loads/boundary conditions and material properties are introduced in the following two subsections.

The stress field of the global model for one load case is also plotted in Fig. 3(a). For all the eight thermo-mechanical load cases, the most highly loaded region along the circumference is the one bolted connection in the vicinity of the lugs, at the lug root.

In the second step of the global-local analysis, the local FE model of the most critical region/bolt, created as part of this program, is shown in Fig. 3(b). 1296 solid elements C3D8R with 8 nodes, one per ply in the thickness direction, are used for the composite flange to detect which ply fails in the composite failure analysis. The aluminum box extracted from the ring is meshed using 720 solid elements C3D8R. The bolt heads are modeled with 102 solid elements C3D8R connected with 10 two-node beam elements B31 representing the bolt shank. Three contact surfaces are established using the hard-contact type, as follows: 1) the surface between the upper bolt-head and the composite flange; 2) the surface between the bottom bolt-head and the aluminum box; 3) the surface between the composite flange and the aluminum box.

The sub-model function in ABAQUS is used to isolate the local structure to be analyzed. It uses automatic splicing to interpolate displacements and stresses at the global-local boundary. Elastic-plastic analysis for the metal part, aluminum part and steel bolts of the local model, is also applied for each load case as shown in Table 1.

3.2 Loads and boundary conditions

Eight thermo-mechanical load cases are provided by Dutch space center. They are combinations of the following loading conditions (for z direction seen in Fig. 3): the minimum temperature (−120 °C); the maximum temperature (100 °C); the maximum tension (F_x=−20.9 kN, F_z=−246 kN); the maximum compression (F_x=+41.8 kN, F_z=+492 kN).

These four loading conditions are made into eight load cases that are applied sequentially, in an attempt to approximate the expected flight scenario. The sequences of load cases are shown in Table 1. For the global model, the applied boundary conditions are zero displacements and rotations for all nodes at the bottom of the ring as shown in Fig. 3(a).

3.3 Material properties

For bolt, as recommended by the Dutch space, the following choices for the bolt parameters are considered in the numerical analysis. Two different bolt sizes, 8 mm (M8) and 10 mm (M10) in diameter are considered. For the M8 bolt, three different preloads are examined: 0, 1.38 and 13.8 kN which is the maximum recommended preload. For the M10 bolt, the maximum recommended preload of 21.9 kN is used. The stress−strain curve used for the steel Hi-Lok bolt is obtained from the handbook [26]. The failure stress of the steel used for the bolt is 1280 MPa.

For composite, the material properties used for the composite cap are given in Table 2, where the subscript z

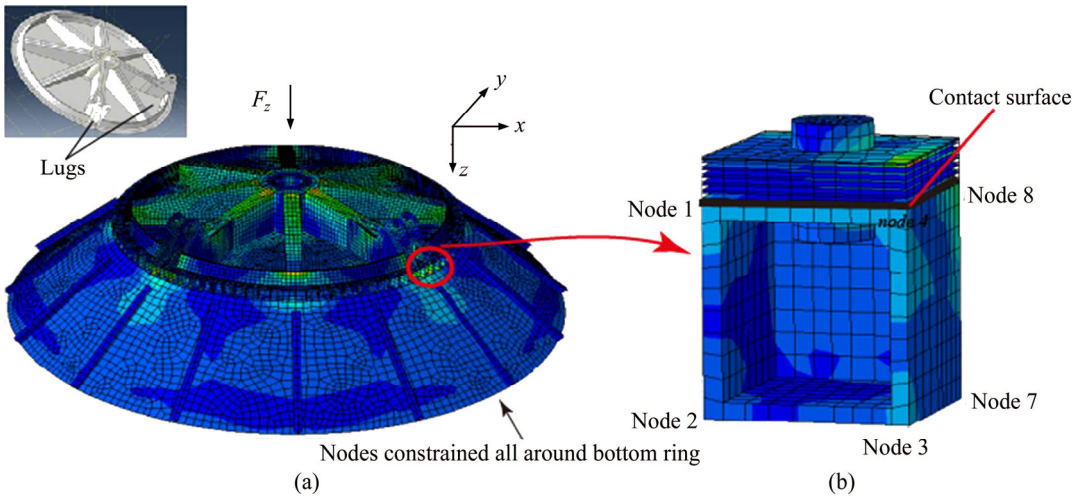

Fig. 3 Sketch of global FE model (upside-down for clarity) (a) and local 3D FE model (b)

Table 1 Applied thermo-mechanical load cases

Load case No.	Condition
1	−120 °C
2	Max tension and −120 °C
3	Max tension and 100 °C
4	Max compression and −120 °C
5	Max compression and 100 °C
6	−120 °C
7	Max tension and 20 °C
8	Max compression and 20 °C

denotes the out-of-plane direction, the superscript t denotes tension and the superscript c denotes compression. X, Y and S denote failure strength values along the warp, fill and shear directions, respectively. There are in total 15 plies in the flange of the composite cap, and the stacking sequence is: $[45_2/0/45/0/45/0/\mathbf{45}]_s$, where the bold denotes that the ply does not repeat on the other side of the mid-plane. For the composite plate, the angle of each ply indicates the direction of the fiber. For example, 45° presents that the fiber of this ply has an angle of 45° respect to the axial direction of the composite plate. The thickness of each ply is given in Table 3.

For aluminum, the stress−strain curve used for the aluminum ring (7075-T651) is obtained from the handbook [26]. The failure stress of the aluminum (7075-T651) is 570 MPa.

4 Results

4.1 Selection of bolt type

Results of the M8 bolt (all three preloads) show the failure of bolts at the critical region in the vicinity of the lug root. In addition to bolt failure, failures of the composite and aluminum parts are also observed. For this reason, the M10 bolt is used. The detailed results presented below in this section are all for the cases of the M10 bolt with the full preload (21.9 kN).

4.2 Boundary conditions at global-local boundary

The use of the sub-model function in ABAQUS guarantees that the displacements at the common nodes of the local and global models match exactly. However, the increased mesh density in the local model will capture stress gradients that the global model will not capture, due to the coarser mesh used. Some differences in the nodal stresses at the common nodes between the global and local model are expected. In this specific case, the differences are relatively small (the largest difference of 25%) and are shown in Table 4. The node numbering is shown in Fig. 3(b).

4.3 Bolt preload

In the local model analysis, we use the maximum recommended preload (21.9 kN) of the M10 bolt. The bolt preload is the initial clamp-up load of the bolt and the bolt clamp-up load always changes under the external load of the structure. In order to determine the actual bolt clamp-up load for different load cases, a contact surface is created at the interface between the upper surface of the aluminum box from the ring and the flange of the composite cap. This is shown as a bold black line in Fig. 3(b). By summing up the interface forces (in z direction), the contact load between composite and aluminum flanges is determined, which is just the bolt clamp-up load under the external load. Positive values of the clamp-up load indicate that the two flanges are in contact. The clamp-up loads for the load cases in Table 1 are shown in Fig. 4. All loads in Fig. 4 are positive, suggesting no separations between the two surfaces.

According to the joint diagrams, when an external tensile force is applied to the joint, it has the effect of reducing some of the clamp force caused by the bolt's preload. It can be seen from Fig. 4 that the clamp-up loads for the load cases featured by tension are much lower than the bolt preload (21.9 kN). The lowest clamp-up load is 2.104 kN for load case 7 which is featured by the maximum tension at room temperature (20 °C). It is reasonable in Fig. 4 that the clamp-up loads for the load cases featured by compression are higher than those for the load cases featured by tension, while at first sight it may seem to be a bit strange that they are also lower than the bolt preload (21.9 kN). However, it should be realized that the deformation of the whole structures caused by the external compression load may produce a tension internal force on the joint. The highest clamp-up load is 12.07 kN for load case 4 which is featured by the maximum compression at −120 °C.

Table 2 Applied load cases

Material property	$E_x=E_y=E_z=60$ GPa	$G_{xy}=G_{xz}=G_{yz}=3.4$ GPa	$v_{xy}=v_{xz}=v_{yz}=0.06$
Failure strength/MPa	$X_t=Y_t=720$	$X_c=Y_c=459$	$S=69.3$

Table 3 Thickness of each ply

Fiber direction/(°)	45	45	0	45	0	45	0	45	0	45	0	45	0	45	45
Thickness/mm	0.286	0.286	0.572	1.144	0.572	1.144	0.572	1.144	0.572	1.144	0.572	1.144	0.572	0.286	0.286

Table 4 Nodal stresses in global and local models at common boundary

Node No.	Nodal stress/MPa		Difference/%
	Global model	Local model	
1	72.22	60.95	15.60
2	28.67	34.97	−21.97
3	28.67	30.89	7.74
4	180.28	198.62	−10.17
5	78.66	70.12	10.85
6	64.96	81.26	−25.09
7	92.22	84.95	7.88
8	70.21	67.25	4.21

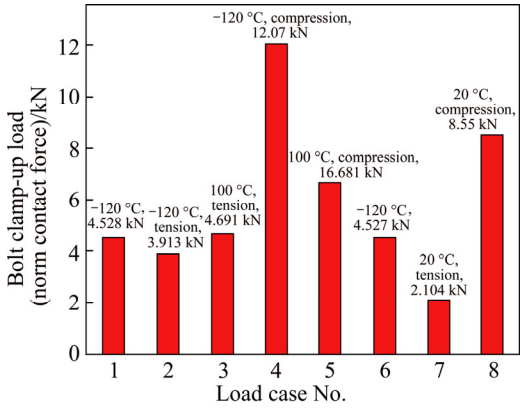

Fig. 4 Bolt clamp-up loads (contact loads) between composite and aluminum flanges

In the bolted connection design, the existence of the clamp-up load indicates that there is no separation between the two connection surfaces; however, it may cause stress concentration if the clamp-up load is too large. This suggests that if other load cases, such as load case 4, are critical because of the preload of 21.9 kN exerted in addition to the loads specified in Table 1, it is possible to relieve the local stresses to make the load cases less critical by reducing the preload up to 2.104 kN or a little less (such that load case 7 just causes separation between the two surfaces).

4.4 Maximum stresses in metal parts

In the local model, the maximum von Misses stresses in the aluminum box and the steel bolt (heads and shank) are shown in Table 5, for each load case with 100% loading. All stresses are below the corresponding failure stresses for the two materials, which is 570 MPa for aluminum and 1280 MPa for steel, and there is no failure. Most of designs can actually support loads somewhat above the ultimate loads (or design loads). The extra load carrying capability is called the margin of safety (MS). Aerospace engineers reported an actual margin of safety which is defined as the percentage of load above the ultimate which can be carried:

Table 5 Maximum von Misses stresses for metal parts by load condition

Load case No.	Condition	Maximum von Misses stress/MPa		
		Aluminum box	Bolt shank (steel)	Bolt head (steel)
1	−120 °C	500.7	306	509.2
2	Max tension and −120 °C	309.2	317	408.3
3	Max tension and 100 °C	301.6	280	466.7
4	Max compression and −120 °C	528.4	317	998
5	Max compression and 100 °C	**561**	**313.4**	**1154**
6	−120 °C	251.8	324.6	538.1
7	Max tension and 20 °C	296.0	325.9	879.2
8	Max compression and 20 °C	500.7	344.5	518.4

$$\mathrm{MS}=\frac{\text{load?capability}}{\text{ultimate?load}}-1 \tag{1}$$

where when the MS reaches a value less than 0, the structure will fail; a margin of 0 means that the structure is predicted to fail at the ultimate loads; a margin of 0.1 means that the structure is predicted to fail at 10% over the ultimate load. In our study, the margin of safety is calculated based on the failure stresses and the maximum von Misses stresses, as follows:

$$\mathrm{MS}=\frac{\sigma_{\text{failure}}}{\sigma_{\text{m}}}-1 \tag{2}$$

where σ_{m} indicates the maximum von Misses stress of the structure and σ_{failure} presents the failure stress of the material. It can be seen from Table 5 that the critical load case is, for both the box and bolt, load case 5 featured by maximum compression and 100 °C. The margins of safety for the metal parts in load case 5 are obtained using Eq. (2), to be:

$$\mathrm{MS}=\begin{cases}0.016\,(1.6\%)\text{ for the aluminum box}\\0.109\,(10.9\%)\text{ for the steel bolt head}\end{cases}$$

which demonstrates that the aluminum box and the steel bolt can still carry margins of safety of 1.6% and 10.9% over the ultimate load presented in Table 1, respectively.

4.5 Failures in composite cap flange

In the local finite element model, since the composite flange is constructed using the solid elements and one element per ply in the thickness direction, the stresses in each ply can be obtained and used as input parameters for composite failure analysis in a Matlab code. For each load case, the in-plane stresses of each element in each ply under the ply coordinate system are

combined in a Tsai-Wu failure criterion [27]:

$$F_1\sigma_1^2 + F_2\sigma_2^2 + F_3\sigma_1\sigma_2 + F_4\sigma_1 + F_5\sigma_2 + F_6\tau_{12}^2 = 1 \quad (3)$$

where

$$F_1 = \frac{1}{X_t X_c},\ F_2 = \frac{1}{Y_t Y_c},\ F_3 = -\sqrt{\frac{1}{X_t X_c}\frac{1}{Y_t Y_c}},$$
$$F_4 = \frac{1}{X_t} - \frac{1}{X_c},\ F_5 = \frac{1}{Y_t} - \frac{1}{Y_c},\ F_6 = \frac{1}{S^2} \quad (4)$$

with local stress σ_1, σ_2, τ_{12} in the ply coordinate system; X_t, X_c, Y_t, Y_c, and S defined in Table 2. If the left hand side of Eq. (3), called Tsai-Wu failure index, is less than 1, there is no failure for this element.

In the local model, the Tsai-Wu failure index of each element in each ply is calculated using Eq. (4) for each load case with a 100% loading. The highest value of the Tsai-Wu failure index for each load case is shown in Table 6. As can be seen from Table 6, the composite cap fails in all cases except load case 7 (with a maximum tension at room temperature). The worst case is load case 4 (with a maximum compression and at −120 °C).

For a state of stress (σ_1, σ_2, τ_{12}) in one layer, the state of stress at failure of the same layer is $S(\sigma_1, \sigma_2, \tau_{12})$, where S is the safety factor for this layer. Substitution of the critical failure state of stress in the Tsai-Wu failure criterion Eq. (3) yields [27]:

$$(F_1\sigma_1^2 + F_2\sigma_2^2 + F_3\sigma_1\sigma_2 + F_6\tau_{12})S^2 + (F_4\sigma_1 + F_5\sigma_2)S - 1 = 0 \quad (5)$$

The corresponding margin of safety is calculated by

$$\mathrm{MS} = \max(S_1, S_2) - 1 \quad (6)$$

where S_1 and S_2 are the two roots of Eq. (5). The highest value of the margin of safety for each load case is shown in Table 6. The margin of safety for load case 4 is −0.3 (−30%). For a linear system this would mean that the applied load should be decreased by a factor 0.7 in order to keep the structure from failure. Since failure here is assumed to coincide with the failure, it is expected to be conservative. The sequence number of the ply where the failed elements locate and the number of the failure element for each load case are listed in Table 6. The failed elements for load cases 1 and 4 in the vicinity of the critical bolt are shown in Fig. 5. Failed elements are outlined in red.

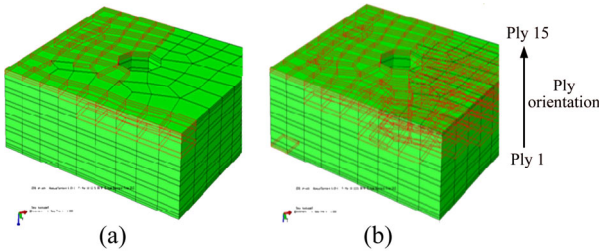

Fig. 5 Failed elements in composite flange for load case 1 (a) and load case 4 (b)

Comparing the Tsai-Wu failure index value and the bolt clamp-up load for each load case in Table 6, it can be concluded that the load case 4 with the largest bolt clamp-up load, is also the most critical case in the composite failure analysis due to the serious stress concentration problem caused by the high clamp-up load. It can be seen from Fig. 5 that the failed elements of the composite cap mainly locate around the bolt hole of the upper surface of the cap. The composite part does not fail in the load case 7, maybe benefitting from the minimum bolt clamp-up load.

5 Improvement for design

Based on the results shown in Section 4, it can be concluded that the composite part is much easier to fail than the metal part in the hybrid composite-to-metal connections. The reason may be that the composite is very prone to delamination failure under the out-of-plane concentrated compression force. The composite cap needs to be improved due to the material failures caused by the high loads presented in the vicinity of the bolts. Alternatives to improve the performance must be considered. These include: increases in the thickness of

Table 6 Composite failure values by load case

Load case No.	Condition	Max Tsai-wu failure index	Max margin of safety	Failure ply by id	Number of failure elements	Bolt clamp-up load/kN
1	−120 °C	2.23	−0.13	11, 13, 14, 15	90	4.528
2	Max tension and −120 °C	1.20	−0.07	11, 13, 14, 15	62	3.913
3	Max tension and 100 °C	1.45	−0.08	11, 13, 14, 15	26	4.691
4	Max compression and −120 °C	5.05	−0.31	1, 9, 11, 13, 14, 15	244	12.07
5	Max compression and 100 °C	1.07	−0.06	14, 15	13	6.681
6	−120 °C	2.23	−0.13	11, 13, 14, 15	90	4.527
7	Max tension and 20 °C	**0.64**	0.03	Non	Non	**2.104**
8	Max compression and 20 °C	2.24	−0.13	11, 13, 14, 15	13	8.55

the composite cap flange, increases in the bolt diameter, and reductions of the preload (seen in Section 4.3). Since the first two methods will increase the weight of the whole structure, which is always avoided in the design of aerospace structures, the way to reduce the preload is used. The results shown in Section 4 are produced using a maximum recommended preload of 21.9 kN for M10 bolt. Since we just need to guarantee that the bolt clamp-up load is not negative, it can be seen from Fig. 4 that the minimum clamp-up load (2.1 kN) in load case 7 is the redundant preload. Based on this conclusion, we consider reducing the preload by 2.1 kN to be 19.8 kN. We then repeat the analysis procedures presented in Section 4 and conclude the results obtained using the new bolt preload as follows:

1) The composite cap and the aluminum ring do not separate under any of the loading conditions.

2) The metal parts, aluminum ring and steel bolt, do not fail.

3) There is no failure in composite part for all load cases.

It can be seen from the above conclusions that the failure of the composite cap flange is mainly caused by the high stress concentration near the bolt, and reducing the bolt preload can improve the situation and reduce the maximum Tsai-Wu failure index of the composite flange.

6 Conclusions and recommendations

1) The differences in the nodal stresses at the common nodes between the global and local model are acceptable, which guarantees that the methodology is correct.

2) The M10 bolt is selected since the bolted connection fails using the M8 bolt.

3) There is no separation between the flanges of the cap and ring for each load case. The minimum bolt clamp-up load is 2.1 kN in load case 7, which can be used as a reference to redesign the bolt preload.

4) The metal parts, the aluminum part and steel bolt, do not fail for each load case. They have positive margins of safety, and the aluminum box and the steel bolt can still carry margin of safety of 1.6% and 10.9% over the design load, respectively.

5) The maximum Tsai-Wu failure index and the maximum margin of safety of the composite part for each load case are calculated using a Matlab code. The composite part fails for all load cases except for one, due to the high loads present in the vicinity of the bolts.

6) In an improved design, the value of the bolt preload is reduced by 2.1 kN from the max preload value of 21.9 kN to guarantee that there is no interface separation in load case 7. The results show that the maximum Tsai-Wu failure index is reduced and the composite part does not fail for each load case. It demonstrates that the unsuitable bolt preload will cause the failure of the composite flange in the hybrid composite-to-metal bolted connections due to the high stress concentration in vicinity of the bolts.

References

[1] LU Yi-yan, HU Ling, LI Shan, WANG Kang-hao. Experimental study and analysis on fatigue stiffness of RC beams strengthened with CFRP and steel plate [J]. Journal of Central South University, 2016, 23(3): 701−707.

[2] GRAHAM D P, REZAI A, BAKER D, SMITH P A, WATTS J F. A hybrid joining scheme for high strength multi-material joints [C]// Proceedings of 18th International Conference on Composite Materials. Jeju, Korea, 2011: 1−6.

[3] UCSNIK S, SCHEERER M, ZAREMBA S, PAHR D H. Experimental investigation of a novel hybrid metal-composite joining technology [J]. Composites Part A: Applied Science and Manufacturing, 2010, 41(3): 369−374.

[4] PARKES P N, BUTLER R, ALMOND D P. Growth of damage in additively manufactured metal-composite joints [C]// Proceedings of 15th European Conference on Composite Materials. Venice, Italy, 2012: 21−29.

[5] PARKES P N, BUTLER R, ALMOND D P. Fatigue of metal-composite joints with penetrative reinforcement [C]// Proceedings of 54th AIAA/ASME/ASCE/AHS/ASC Structures, Structural Dynamics and Materials Conference. Boston, USA, 2013: 1−9.

[6] SUN H T, CHANG F K, QING X L. The response of composite joints with bolt-clamping loads, part II: Model verification [J]. Journal of Composite Materials, 2002, 36(1): 47−67.

[7] CACCESE V, BERUBE K A, FERNANDEZ M, MELO J D, KABCHE J P. Influence of stress relaxation on clamp-up force in hybrid composite-to-metal bolted joints [J]. Composite Structures, 2009, 89(2): 285−293.

[8] CACCESE V, MEWER R, VEL S S. Detection of bolt load loss in hybrid composite/metal bolted connections [J]. Engineering Structures, 2004, 26(7): 895−906.

[9] PARKES P N, BUTLER R, MEYER J, OLIVEIR A D. Static strength of metal-composite joints with penetrative reinforcement [J]. Composite Structures, 2014, 118(1): 250−256.

[10] STARIKOV R, SCHON J. Experimental study on fatigue resistance of composite joints with protruding-head bolts [J]. Composite Structures, 2002, 55(1): 1−11.

[11] KELLY G. Quasi-static strength and fatigue life of hybrid (bonded/bolted) composite single-lap joints [J]. Composite Structures, 2006, 72(1): 119−129.

[12] QIN Xun-peng. Modelling and simulation of contact force in cold rotary forging [J]. Journal of Central South University, 2014, 21(1): 35−42.

[13] CAO Qiang, HUA Lin, QIAN Dong-sheng. Finite element analysis of deformation characteristics in cold helical rolling of bearing steel-balls [J]. Journal of Central South University, 2015, 22(4): 1175−1183.

[14] CARTIE D D R, COX B N, FLECK N A. Mechanisms of crack bridging by composite and metallic rods [J]. Composites Part A: Applied Science and Manufacturing, 2004, 35(11): 1325−1336.

[15] NOGUEIRA A C, DRECHSLER K. Analysis of the static and fatigue strength of a damage tolerant 3D reinforced joining technology on composite single lap joints [C]// Proceedings of 53rd AIAA/ASME/ASCE/AHS/ASC Structures, Structural Dynamics and Materials Conference. Hawaii, USA, 2012: 1−6.

[16] IREMAN T. Three-dimensional stress analysis of bolted single-lap composite joints [J]. Composite Structures, 1998, 43(3): 195−216.

[17] TSERPES K I, LABEAS G, PAPANIKOS P, KERMANIDIS T. Strength prediction of bolted joints in graphite/epoxy composite laminates [J]. Composites Part B: Engineering, 2002, 33(7): 521−529.

[18] HUHNE C, ZERBST A K, KUHLMANN G, STEENBOCK C, ROLFES R. Progressive damage analysis of composite bolted joints with liquid shim layers using constant and continuous degradation models [J]. Composite Structures, 2010, 92(2): 189−200.

[19] KAPANIA R K, HARYADI S G, HAFTKA R T. Global/local analysis of composite plates with cutouts [J]. Computational Mechanics, 1997, 19(5): 386−396.

[20] REINOSO J, BLAZQUEZ A, ESTEFANI A, PARIS F, CANAS J. A composite runout specimen subjected to tension–compression loading conditions: Experimental and global–local finite element analysis [J]. Composite Structures, 2013, 101(15): 274−289.

[21] REINOSO J, BLAZQUEZ A, ESTEFANI A, PARIS F, CANAS J, ARVALO E, CRUZ F. Experimental and three-dimensional global/local finite element analysis of a composite component including degradation process at the interfaces [J]. Composites Part B: Engineering, 2012, 43(4): 1929−1942.

[22] JRAD M, SUNNY M R, KAPANIA R K. Global–local analysis of composite plate with thin notch [J]. Journal of Aircraft, 2014, 51(3): 967−974.

[23] BOGDANOVICH A E, KIZHAKKETHARA I. Three-dimensional finite element analysis of adhesively bonded plates [C]// Proceedings of 38th AIAA/ASME/ASCE/AHS/ASC Structures, Structural Dynamics and Materials Conference. Kissimmee, FL, USA, 1997: 1984−1992.

[24] BOGDANOVICH A E, KIZHAKKETHARA I. Three-dimensional finite element analysis of double-lap adhesive bonded joints using submodeling approach [J]. Composites Part B: Engineering, 1999, 30(6): 537−551.

[25] LIU Yan-jie, SUN Qin, FAN Xue-ling. A non-intrusive global/local algorithm with non-matching interface: Derivation and numerical validation [J]. Computer Methods in Applied Mechanics and Engineering, 2014, 277(2): 81−103.

[26] Metallic materials and elements for aerospace vehicle structures [M]. Department of Defense, 1994, 2: 103−106.

[27] BAKKER M. Stress fields around bolts in bolted joints and trends for failure predictions [D]. Delft: Delft University of Technology, 2012.

(Edited by YANG Hua)

Cite this article as: LIANG Ke. A global-local finite element analysis of hybrid composite-to-metal bolted connections used in aerospace engineering [J]. Journal of Central South University, 2017, 24(6): 1225−1232. DOI: 10.1007/s11771-017-3526-5.